Original Article

Journal of Intelligent Material Systems and Structures

Journal of Intelligent Material Systems and Structures 2021, Vol. 32(20) 2529–2540 © The Author(s) 2021 Article reuse guidelines: sagepub.com/journals-permissions DOI: 10.1177/1045389X211006906 journals.sagepub.com/home/jim



# Partially activated reconfigurable arrays to guide acoustic waves

Ningxiner Zhao<sup>1</sup>, Chengzhe Zou<sup>1</sup> and Ryan L Harne<sup>2</sup>

### **Abstract**

Recent studies have exemplified the potential for curved origami-inspired acoustic arrays to focus waves. Yet, reconfigurable structures that adopt curvatures are often difficult to translate to practice due to mechanical deformation of the facets that inhibit straightforward folding. In addition, not all tessellations that curve upon folding are also flat-foldable, which is a key advantage of portability inherent to many origami-inspired structures. This research introduces a new concept of partially activated reconfigurable acoustic arrays as a means to mitigate these drawbacks. Here, tessellations are studied where a subset of the facet surfaces are considered to radiate acoustic waves. The analytical results reveal focusing behaviors in such arrays that are otherwise not manifest for the array when fully activated. The focused waves are more intense in amplitude and space for partially activated arrays than fully activated counterparts. These trends are verified by experiment and are also found to be applicable to multiple reconfigurable array geometries. The results encourage broader study of the design space accessible in reconfigurable arrays to capitalize on all of the functionality afforded by origami-inspired wave guiding structures.

### **Keywords**

Origami, acoustic arrays, reconfigurable structures

### I. Introduction

Origami-based structures are under close investigation throughout science and engineering because of the extreme portability and reconfigurability afforded in an easy-to-manufacture platform. The concept of origami is introduced in numerous fields, including for soft robots, metamaterials, and programmable structures (Babaee et al., 2016; Bertoldi et al., 2017; Boatti et al., 2017; Lv et al., 2014; Martinez et al., 2012; Overvelde et al., 2016; Rus and Tolley, 2018; Silverberg et al., 2014). Mechanical manipulators (Belke and Paik, 2017; Miyashita et al., 2017) and biomedical devices (Johnson et al., 2017; Kuribayashi et al., 2006) also leverage the versatility of origami principles to modulate mechanical properties and function in accordance with the application need.

In addition, the advantages of origami concepts are finding outlets in practices of wave guiding. Conventional digital control over the amplitude and phase of transducer elements in acoustic and radio frequency arrays is intended to emulate the physical redistribution of transducers to focus and steer beams of waves (Balanis, 2016; Williams, 1999). By exhibiting large and reversible change of shape with few folding actions (Tachi, 2010), origami-inspired arrays enable a mechanical control over wave propagation that is not

susceptible to challenges inherent to digital control techniques (Harne and Lynd, 2016). Alharbi et al. (2018) examined origami-inspired reconfigurable dipole antennas composed of e-textiles for applications involving wearable communication systems, while Liu et al. (2015) and Yao et al. (2017) studied spiral-shaped antennas that folded to adapt RF properties. Frequency selective surfaces created from reconfigurable origami structures have also been investigated as means to adapt RF wave transmission and radiation (Fuchi et al., 2012; Sessions et al., 2018). Similar adaptation has been achieved for arrays composed of acoustic transducers for sake of steering and modulating acoustic fields (Bilgunde and Bond, 2018; Zou et al., 2018).

#### Corresponding author:

Ryan L Harne, Department of Mechanical Engineering, The Pennsylvania State University, 336 Reber Building, University Park, PA 16802-4400, USA.

Email: ryanharne@psu.edu

Department of Mechanical and Aerospace Engineering, The Ohio State University, Columbus, OH, USA

<sup>&</sup>lt;sup>2</sup>Department of Mechanical Engineering, The Pennsylvania State University, University Park, PA, USA

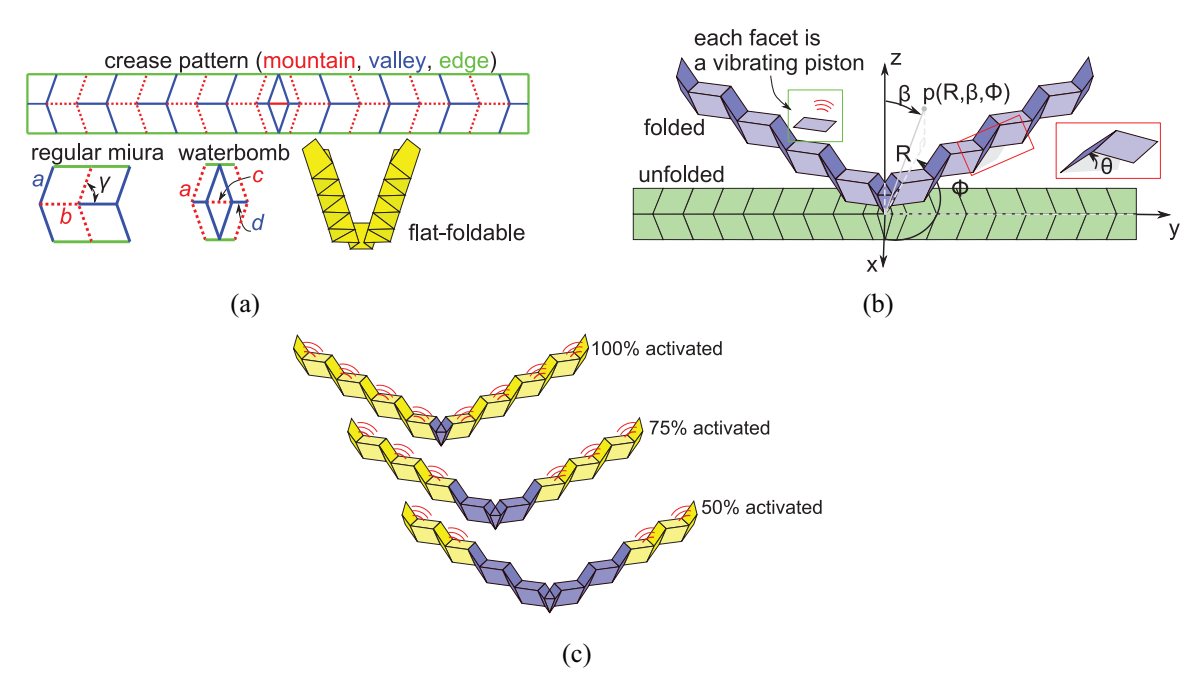


Figure 1. (a) Folding pattern and geometric parameters of the flat-foldable tessellated array, (b) folded and unfolded configurations, and the point locations in the acoustic field, and (c) exemplary illustrations of partial activation promoting better waves focusing by minimizing destructive interference effects.

Focusing acoustic waves is central to numerous applications including the ablation of solid tumors (Illing et al., 2005; Kennedy, 2005), nondestructive testing (Drinkwater and Wilcox, 2006), and industrial (Harker et al., 2014) and biomedical imaging (Fink et al., 2003). In high-intensity focused ultrasound practices, the acoustic waves converge at the focal point where the tumor is ablated. Consequently, curved transducers are employed (Kennedy, 2005). Yet, it is difficult to access the tumor locations for cancers deep in the body and thus challenging to ablate tumors inaccessible by conventional large probes. Recent studies have proposed using origami-inspired transducers that fold flat for transport through the body to the point of care, whereafter the unfolded transducer focuses ultrasound at the tumor for treatment, followed by a reversal of the process to exit the body (Zou et al., 2018). Yet, the curved origami transducer surfaces proposed for such vision are not flat-foldable (Zou and Harne, 2017; Zou et al., 2018). Although there are flat-foldable origami structures able to realize curved forms (Dudte et al., 2016), the tessellations are not easily held in position in practice due to elastic deformation of the facet surfaces (Schenk and Guest, 2011). On the other hand, regular non-curved and flat-foldable tessellations such as the regular Miura-ori (Schenk and Guest, 2013) are easy to maintain in precise folded configurations due to the in-plane kinematic reconfiguration. Unfortunately, when outfit with acoustic transducers, acoustic arrays established on regular Miura-ori patterns do not focus acoustic waves (Harne and Lynd, 2016; Zou and Harne, 2018).

Motivated by these shortcomings, the goal of this research is to devise and study an acoustic array based on the regular Miura-ori tessellation that focuses waves according to the folded configuration. The proposed technique to realize focused waves with a traditionally non-focusing array structure is based on partial activation of the acoustic transducers positioned on a piecewise assembled folding structure. The crease pattern and geometric parameters of the tessellated array studied here are shown in Figure 1(a). A waterbomb unit is used at the center of the array to enable folding of two arms each composed from four regular Miura-ori units. The regular Miura-ori units are considered to vibrate like baffled pistons and thus to radiate acoustic waves, Figure 1(b). The hypotheses tested in this report are that (1) the folded array from regular Miura-ori surfaces focuses waves and (2) the partial activation of the array leads to more dramatic focusing. The first hypothesis is supported on the intuition that the Vshape realized by the folded array, Figure 1(b), may lead to converging waves along the z axis. The second hypothesis is exemplified in Figure 1(c). When all eight Miura-ori units are activated to radiate waves, there may be less constructive interference of waves along the the z axis than when only 75% of the units are activated. Conversely, when only 50% of the units are

activated, greater constructive interference may occur along the z axis to focus waves. Consequently, this research investigates the efficacy of partial activation of the flat-foldable and piecewise assembled array, Figure 1(a), to focus waves while retaining the simplicity of array reconfiguration by exploiting the regular Miura-ori tessellation.

This research undertakes analytical and experimental efforts to scrutinize the wave focusing opportunities afforded by partially activated acoustic arrays. Section 2 presents the analytical model composed to study the wave guiding characteristics of the arrays. Then, Sec. 3 details theoretical investigations undertaken to explore the parametric influences of array design, folding extent, and partial activation. An extension of the concept to another acoustic array is also provided to exemplify the robustness of the proposed concept. Sec. 4 reports experimental efforts to validate the key discoveries of the analytical investigations. Finally, the new findings are summarized with concluding remarks.

# 2. Analytical model

## 2.1. Model formulation

The structural and acoustic geometries of the partially activated arrays collectively influence the wave focusing capabilities. In order to predict the focusing behavior of the acoustic array, Rayleigh's integral is used in this research to study the relationship among these parameters (Zou and Harne, 2018). Rayleigh's integral assumes the vibrating planar surface under study is baffled so that acoustic pressure radiates away from the vibrating surface only in one direction. This assumption is satisfied in the subsequent experimental validation as described in Sec. 4.1. Recent research has furthermore characterized the relative contributions of reflected and diffracted waves from adjacent vibrating baffled surfaces oriented at oblique angles (Zou and Harne, 2019), which helps to illuminate that only for small angles between the adjacent surfaces is Rayleigh's integral alone insufficient for prediction. This indicates that the following analytical modeling formulation is sufficiently accurate to predict wave focus capability when the array is not significantly folded, such as nearly folded flat.

The geometries of the regular Miura-ori units and the central waterbomb unit are shown in Figure 1(a). The topology of the regular Miura-ori unit is defined for unfolded and folded configurations by four parameters: edge lengths a and b, edge angle  $\gamma$ , and folding angle  $\theta$  (Schenk and Guest, 2013). The facets of the Miura-ori units are assumed to vibrate like baffled pistons. Rayleigh's integral is employed to characterize the acoustic field produced by the array. The acoustic pressure p is defined at a field point in a spherical coordinate system using the radial distance R, elevation

angle  $\beta$ , and azimuth angle  $\phi$ . The origin is at the geometric center of the unfolded tessellated array, Figure 1(b). For the tessellation studied here, the Rayleigh's integral (Williams, 1999) is computed from the superposition of contributions from all facet areas activated and vibrating. The total acoustic pressure at the field point is therefore

$$p(R, \beta, \phi, t) = j \frac{\rho_0 \omega u_0}{2\pi} e^{j\omega t} \sum_{n=1}^{N} \left[ \int_{A_n} \frac{e^{-jkR_n}}{R_n} dA_n \right]$$
(1)

Here, the  $\rho_0$  is the density of the fluid medium,  $\omega$  is the angular frequency and  $u_0$  is the amplitude of the normal particle velocity of the vibrating facet, N is the number of facets,  $A_n$  is the area of the  $n^{th}$  facet,  $k = \omega/c_0$  is wavenumber where  $c_0$  is sound speed,  $R_n$  is the distance from the center of the  $n^{th}$  facet to the field point. In this study, air is the fluid medium so that  $\rho_0 = 1.21 \text{ kg/m}^3$  and  $c_0 = 343 \text{ m/s}$ .

The equation (1) is only able to be resolved analytically for the far field, that is for field points many acoustic wavelengths away from the array surface (Williams, 1999). As a result, to determine nearfield acoustic pressure to study the wave focusing ability of the arrays, the technique developed by Ocheltree and Frizzell (1989) is employed. The technique, often used in studies of ultrasonic transducers (Ebbini and Cain, 1991; Jensen and Svendsen, 1992; Ross et al., 2005; Wan et al., 1996), involves finely discretizing the soundradiating surfaces to such small modeled dimensions that the nearfield points are in the acoustic far field of each discretized facet surface. The resulting superposition of all discretized surface contributions then enables the computation of the nearfield and far field waves projected from the array. The discretized version of the Rayleigh's integral used here, inspired by this technique, is given in equation (2) where  $A_{mn}$  is the  $m^{th}$  discretized surface element on the  $n^{th}$  facet and M is the number of discretized surfaces on a given facet.

$$p(R, \beta, \phi, t) = j \frac{\rho_0 \omega u_0}{2\pi} e^{j\omega t} \sum_{n=1}^{N} \sum_{m=1}^{M} \left[ \frac{e^{-jkR_{mn}}}{R_{mn}} A_{mn} \right]$$
(2)

In the following research, this approach is iterated during convergence study to identify a sufficient refinement of each facet so that near field predictions converge. Here, 512 elements are created over each facet surface to lead to accurate and converged near field predictions of the acoustic wave focusing phenomena. The sound pressure level (SPL) is then found using

$$SPL = 20\log_{10} \left[ \frac{p_{rms}(R, \beta, \phi)}{p_{ref}} \right]$$
 (3)

The  $p_{rms}(R, \beta, \phi)$  is the root mean square value of  $p(R, \beta, \phi)$ , while  $p_{ref} = 20 \mu Pa$  is the reference acoustic pressure in air. When examining partially activated

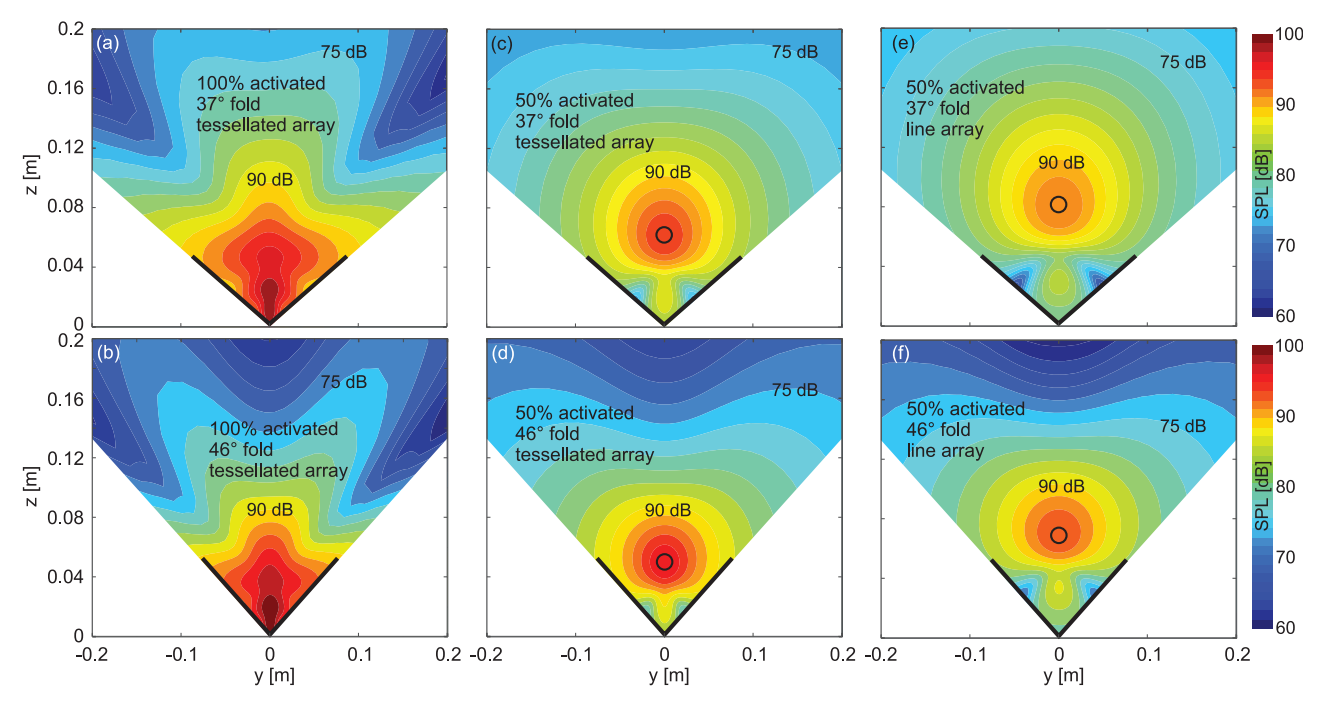


**Figure 2.** Near field wave focusing from tessellated and ideal folded line acoustic arrays: (a, c, and e) SPL in the y-z planes for the arrays folded to 37°, (b, d, and f) SPL for arrays folded to 46°. Frequency of array activation is 15 kHz. The white space denotes regions not accessible to prediction by the modeling formulation. The thick black angled lines at the bottom of the shaded space denote the nominal linear cross-section of the respective array. The black circles in (c–f) denote the focal points.

arrays, the sum over the facets in equation (2) accounts only for the active facets considered to radiate waves.

# 2.2. Theoretical assessment of the partial activation hypotheses

To provide a first test for the two hypotheses of this research that (i) the piecewise assembled arrays of regular Miura-ori focus sound and that (ii) the partially activated arrays lead to greater wave focusing, Figure 2(a) and (c) compare the sound pressure level (SPL) in the y - z plane for tessellated arrays utilizing activation constituting 100% and 50% of the surface when driven at 15 kHz and folded to  $\theta = 37^{\circ}$ . The unshaded areas correspond to locations where Rayleigh's integral cannot be computed on the basis of the modeled baffled sound radiating surfaces. The thick black angled lines at the bottom of the shaded space denote the nominal linear cross-section of the respective array. The arrays have dimensions of a = 7 mm, b = 7 mm,  $\gamma = 70^{\circ}$ , c = 8 mm, d = 5 mm. Compared with the fully activated tessellated array in Figure 2(a), the array in Figure 2(c) that is activated on the 50% of the folded Miura arms most distant from (y, z) = (0, 0) shows distinct wave focusing around z = 0.6 m. Similar trends are identified when the arrays are folded to  $\theta = 46^{\circ}$  in Figure 2(b) and (d). It is further seen in Figure 2(b) that the fully activated array projects high levels of sound to the near field without dramatic focusing effect at a defined focal point. Focusing necessitates spatial localization of acoustic waves (O'Neil, 1949), indicating that the results in Figure 2(a) to (d) exemplify that only the partially activated array achieves a focusing capability. While further studies reported in the Sec. 3 of this report investigate spectral and geometric influences to the focusing capability, these preliminary findings help motivate the subsequent detailed investigation.

To assess the distinctions between the tessellated, partially activated array and an ideal line array that is likewise partially activated and folded in half, Figure 2(e) and (f) shows the results of the SPL in the near field for a folded line array driven at 15 kHz and folded to angles 37° and 46°, respectively. The SPL predictions for the line array may be computed directly from derived relations for the sound radiation from lineshaped acoustic sources (Kinsler et al., 2000) accounting for the relative rotation between linear strips, or may be computed through the analytical approach adopted here. The width and length of the unfolded line array are the same as those for the tessellated array: 13.1 mm wide and 112 mm long. As seen in Figure 2(e) and (f), the focal point for the partially activated line array is further from the array center (v,z) = (0,0)than for the tessellated array in Figure 2(c) and (d). This is intuitive because the tessellation includes facets partially facing toward z = 0. This means that the resulting constructive interference occurs closer to (y,z) = (0,0) for the tessellated array than for the

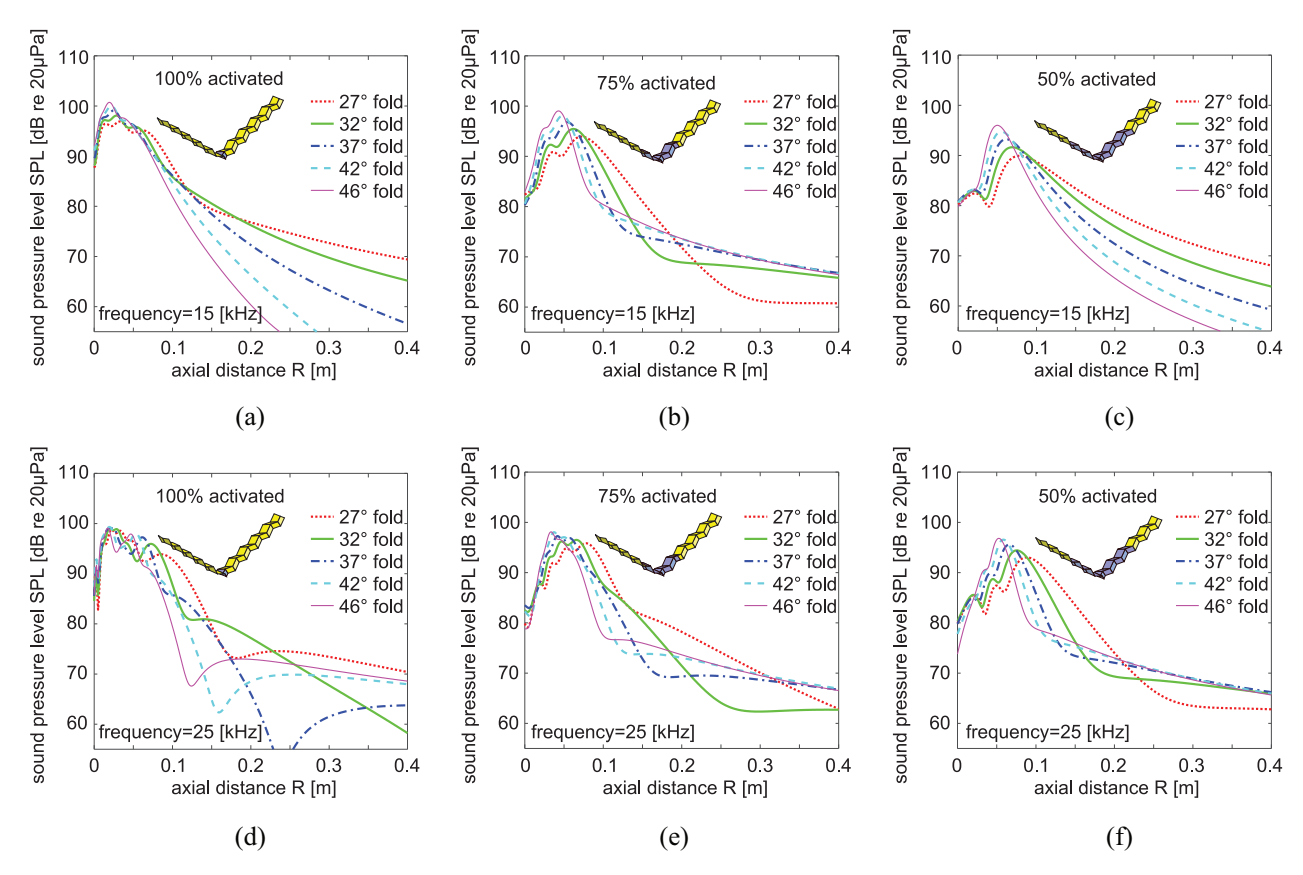


**Figure 3.** Folding influence on wave focusing. SPL along the z axis at 15 kHz for arrays that are: (a) 100% activated, (b) 75% activated, and (c) 50% activated. Corresponding results at 25 kHz for (d) 100%, (e) 75%, and (f) 50% activated arrays. In each sub-figure, the folding angles considered are  $27^{\circ}$ ,  $32^{\circ}$ ,  $37^{\circ}$ ,  $42^{\circ}$ , and  $46^{\circ}$ . The insets illustrate the activation percentage and partially folded array.

nominal line array. In addition, the focal point SPL for the partially activated tessellated array is greater than the focal point SPL for the corresponding line array. For the folding angles of 37° and 46°, the focal point SPL is 93 and 96 dB for the tessellated array, whereas the nominal folded line array provides 89 and 92 dB to the focal points under the same fold extents. Such advantage for focusing by the tessellated array may be attributed to the facets that point toward the v axis once folded, as observed in Figure 1(b). Further model validation is provided in Sec. 4 to fully establish the efficacy of the new modeling tool. Yet these first results are sufficient to support the hypotheses of this research and test the modeling predictions against known analytical solutions for idealized sound radiating surfaces like the line. The following sections then seek to shed broad light on the parametric influences that culminate in adaptive sound focusing capability from partially activated and tessellated acoustic arrays.

## 3. Studies and discussions

In this section, the analytical model is employed to characterize wave focusing from the piecewise assembled and partially activated acoustic array. The studies give attention to focusing capability, frequency sensitivities, and extensibility of the principle.

# 3.1. Enhancement of wave focusing by folding partially activated arrays

In Sec. 3.1 and 3.2, the array studied consists of two arms having five regular Miura-ori units and one central waterbomb unit. The dimensions of the array are a = b = 8 mm,  $\gamma = 70^{\circ}$ , c = 8 mm, d = 5 mm.

Figure 3(a) to (c) respectively present results of the SPL at 15 kHz along the z axis when the activation of the array surface is over 100% of the Miura-ori units, over 75%, and over 50%. In each sub-figure, the line styles indicate different extents of folding of the array, while the insets show the array when folded to  $\theta = 25^{\circ}$ . In these examples, as the folding angle increases, the peak value of the axial SPL uniformly increases while the focal point location concurrently draws closer to the array center at R = 0. Both trends are intuitive because the more highly folded arrays may direct sound to focal points nearer to the array center and will do so at higher amplitudes of acoustic pressure due to

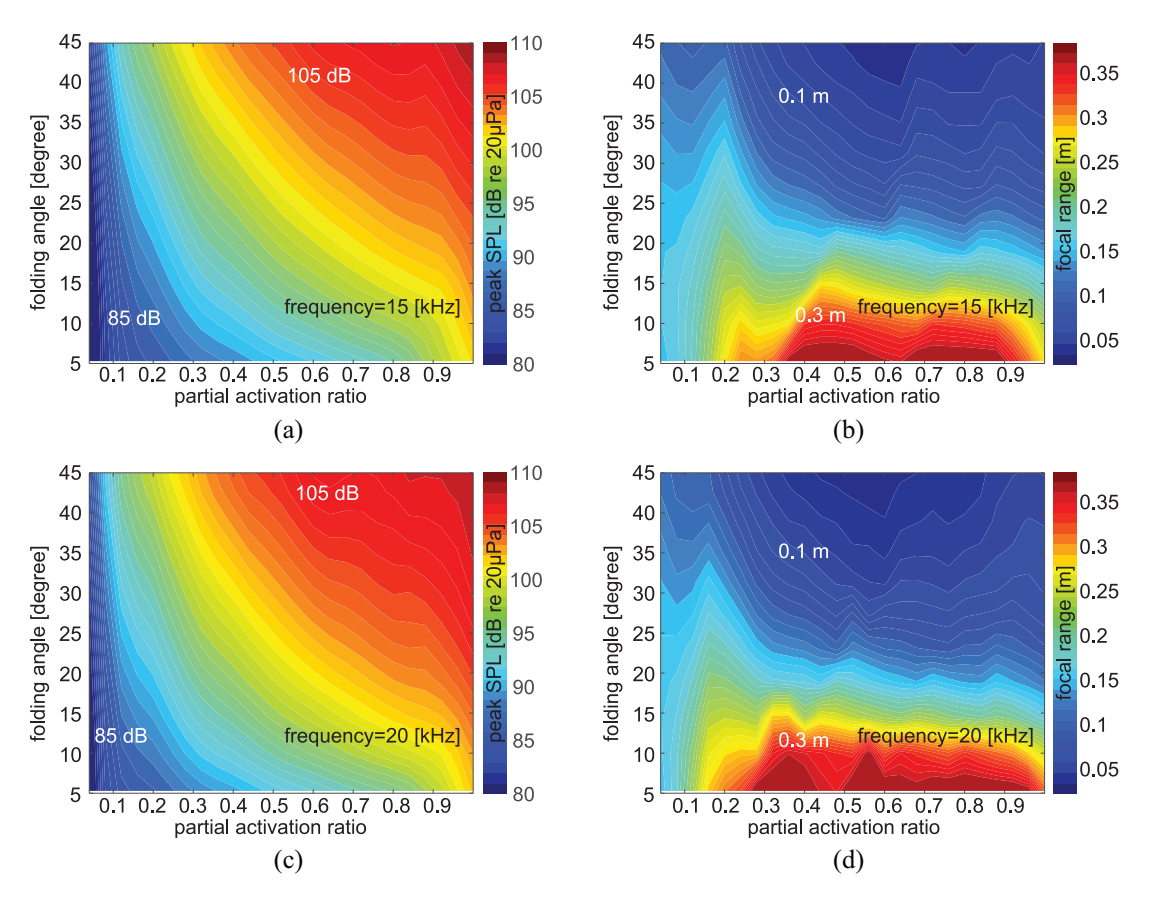


Figure 4. (a, c) SPL at the focal point as a function of partial activation ratio and folding angle and (b, d) focal range as a function of partial activation ratio and folding angle. The driving frequencies are 15 kHz in (a, b) and 20 kHz for (c, d).

reduced distance of travel on the basis of geometric acoustics (O'Neil, 1949). The same trends are confirmed for the driving frequency of 25 kHz, for the results shown in Figure 3(d) to (f). Considering the findings of Figure 3, the more highly folded and less activated arrays lead to focal points that are more defined than the less folded and fully activated counterparts.

Similar to the preliminary results in Figure 2, Figure 3(a) to (c) confirm that the reduction of array activation percentage leads to a focal point shift away from the array center, thus to greater axial distance. A more spatially confined focal range is also observed with reduction of the array activation. The focal range is the range of axial distance over which the sound pressure level (SPL) is no more than 6 dB less than peak SPL at the focal point. One may relate this trend to the greater similarity between the classical half-circle (or arc) radiator of sound and the present tessellated array when only 50% of the surfaces are activated than when all 100% of the surfaces are activated. On this basis, these results suggest that despite lacking an inherent curvature preferred to focus waves, tessellated arrays that sufficiently reproduce curvatures by the activated surfaces result in more substantial focusing effects.

These trends are more comprehensively characterized in Figure 4. Figure 4(a) and (c) present the SPL at the focal point as a function of the partial activation ratio and the folding angle for frequencies 15 and 20 kHz, respectively. At both frequencies, increasing activation ratio or folding angle results in greater peak SPL. The explanations for these findings are apparent. Greater activation of the surfaces leads to larger net activated area and thus more absolute pressure radiated to the focal point. Also, the more highly the array is folded, the closer the wave-radiating surfaces are to the z axis, which likewise may lead to greater focal point SPL.

Figure 4(b) and (d) further characterize the results in terms of the focal range. Here, the focal range is defined as the axial distance range over which the SPL is no more than 6 dB less than the focal point peak SPL. The results in Figure 4(b) and (d) reveal that increasing the array folding angle reduces the focal range. Reduced focal range indicates a more substantial focusing effect since a sharply defined focal point is often sought in applications of ultrasound ablation of tumors and targeted communications. For a given folding angle such as around 35°, the reduction of

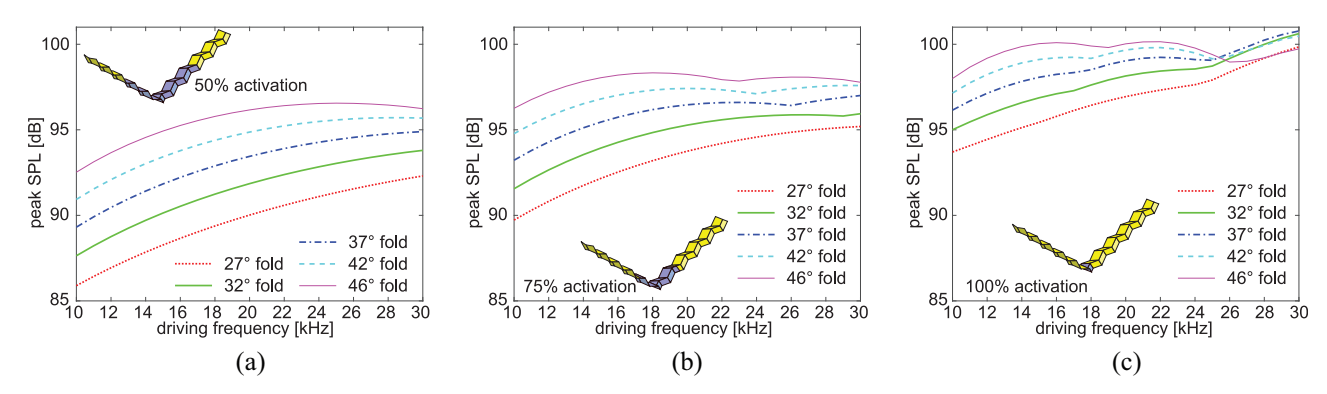


Figure 5. SPL at the focal point as a function of the driving frequency of the tessellated array. Arrays activated over: (a) 50% area of Miura-ori unit, (b) 75% area, and (c) 100% area. Linestyles correspond to folding angle extent of the arrays.

activation ratio causes the focal range to change in a nonlinear way. Specifically, for both 15 and 20 kHz in Figure 4(b) and (d) with arrays folded to 35°, the focal region is higher in value, then lesser in value, and then higher in value again with the increase of activation ratio. Between Figure 4(b) and (d), the specific partial activation ratio that most reduces the focal range is not the same. For 15 kHz in Figure 4(b), the smallest focal range is found for 35° when the partial activation ratio is around 0.60, where for 20 kHz in Figure 4(d) the smallest focal range occurs for 0.55 activation ratio. These results suggest that an optimal partial activation percentage exists for the array under a given folding extent and driving frequency of operation.

### 3.2. Influence of driving frequency on beak axial SPL

The trends uncovered in Sec. 3.1 indicate the piecewise assembled and partially activated flat-foldable acoustic arrays may focus sound at two specific frequencies. Here, the frequency sensitivity of these trends is investigated. The focal point SPL as a function of frequency is presented in Figure 5. From Figure 5(a) to (c), the partial activation percentage changes from 50% to 75% and then to 100%. Figure 5(a) and (b) both suggest that the increased folding of the arrays uniformly increase the focal point SPL. Similarly, in both cases of partial activation percentage 50% and 75%, the increase of frequency increases the focal point SPL. This latter trend agrees with the principle of Rayleigh's integral equation (1) that for increasing frequency with constant amplitude of surface normal velocity, the acoustic pressure amplitude increases. Comparatively, when the array is fully activated in Figure 5(c), the SPL shows a strong frequency dependence above 26 kHz for folding angles 42° and 46°. Because the wave radiating surfaces of the Miura-ori units are not directly and identically pointed to a common focal point, destructive interference may occur when the wavelengths are on the order of the facet dimensions such as at frequencies greater than

26 kHz for the fully activated tessellated array. The results of Figure 5 indicate that the partially activated arrays, especially the array activated over just 50% of the Miura-ori units, are less susceptible to destructive interference effects for focusing acoustic waves.

# 3.3. Extension of partial activation principle to composite tessellated array

The studies in Secs. 3.1 and 3.2 conclude that piecewise assembled and partially activated tessellated arrays enable wave focusing by improving constructive interference effects within a defined focal region. According to these findings, the percentage of the partially activated surfaces is central to assist in the focusing effect of the piecewise assembled Miura-ori acoustic array. To test the extensibility of the concept, here another tessellation is considered for the efficacy of partial activation to aid in focusing effects.

Here, the square twist is considered as another tessellation platform on which an acoustic array is established. The crease pattern of the square twist is shown in Figure 6(a). The tessellation consists of five squares and four parallelograms. The dimensions considered are: a=32.3 mm,  $\alpha=30^{\circ}$ , as shown in Figure 6(a). Figure 6(b) shows the folded and unfolded version of the array. As before, the tessellation is considered to have facets that vibrate like baffled pistons over the activated surfaces. Figure 6(c) shows three folding states that are examined. Fold 1 is the least folded whereas fold 2 and 3 are progressively more folded.

Figure 6(d) and (e) respectively contrast the axial SPL of the fully activated square twist and of the square twist when only square facets are activated. In Figure 6(d) at 20 kHz, there are no observable focusing effects for the fully activated array. In comparison, a clear trend of focused waves occurs around an axial distance of 0.01 m in Figure 6(e) for the partially activated square twist array. The peak SPL in Figure 6(e) is more than 8 dB the peak amplitude of SPL in Figure 6(d),

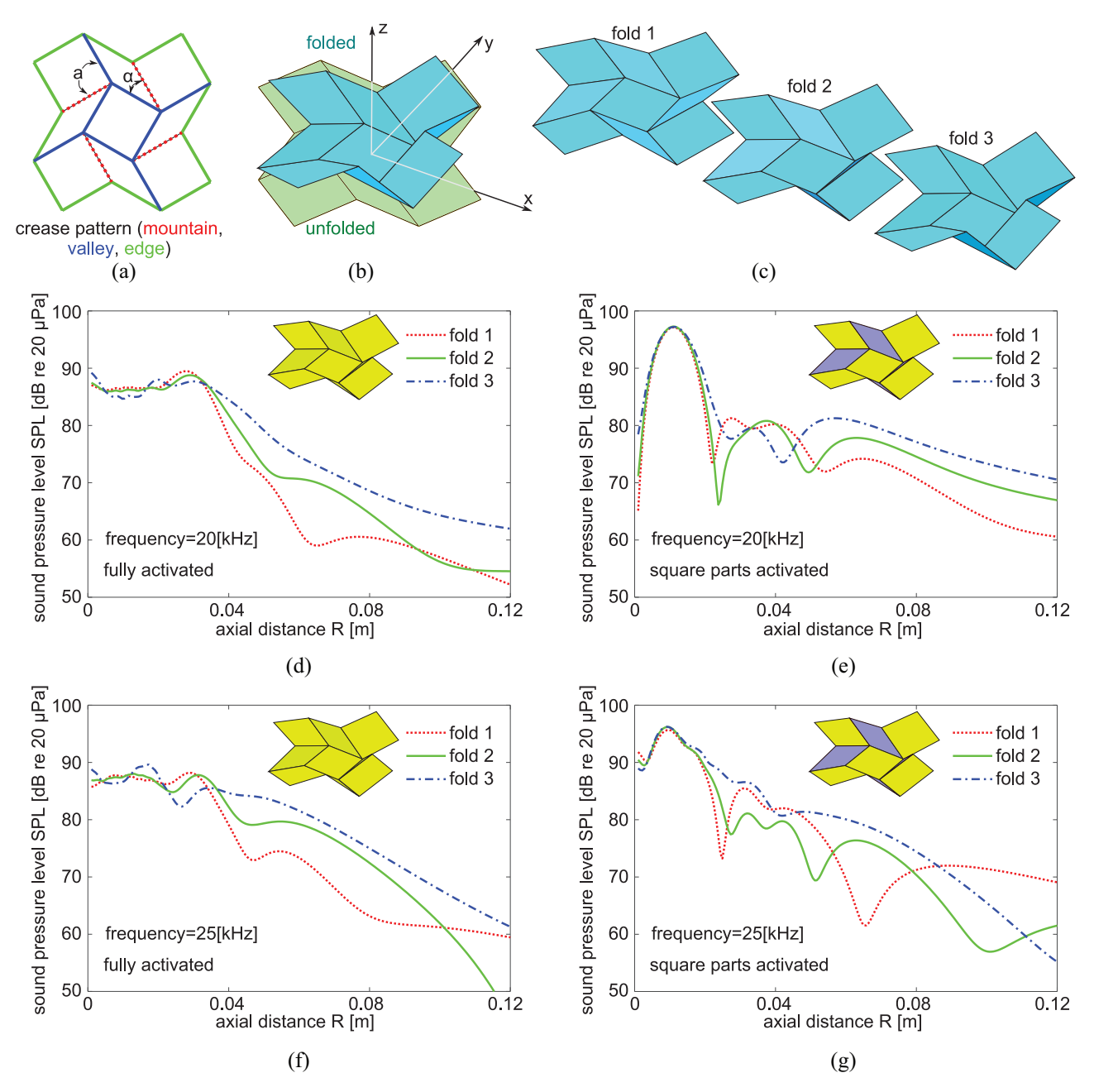


**Figure 6.** Overview of square twist array: (a) crease pattern, (b) illustration of the folded and unfolded array geometries with respect to the central z axis for focusing, (c) three folding states of the square twist array, (d and f) SPL as a function of axial distance and folding extent for the fully activated array, and (e and g) for the array when only square facets are activated. Driving frequencies are 20 kHz for top row and 25 kHz for bottom row.

emphasizing the advantage of the partial activation approach. These results are underscored in Figure 6(f) and (g) for the case of 25 kHz: a focusing behavior is observed when the array is partially activated Figure 6(f), whereas no focusing is induced for the fully activated array. All together, these findings demonstrate the extensibility of the partial activation approach to

create wave focusing capabilities in acoustic arrays that do not focus sound when fully activated.

# 4. Experimental validation

A tessellated array specimen is fabricated and experiments are undertaken to test the feasibility of the partial

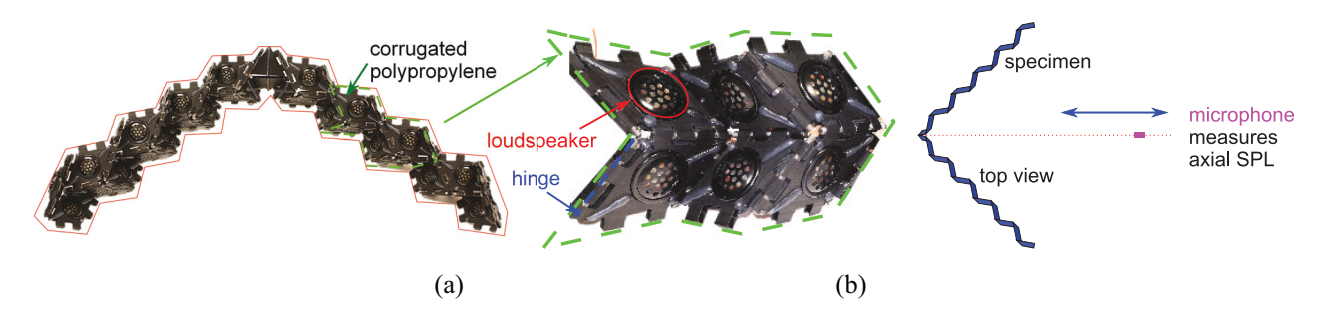


**Figure 7.** Overiew of the specimen and experiment setup: (a) the assembly of the specimen, made of corrugated polypropylene, loudspeakers and hinges. Four regular Miura-ori units are used on each side of the central waterbomb unit and (b) top view schematic of the experiment setup, a microphone is used to measure the axial SPL.

activation approach to translate to a practical example. Experimental and analytical results are gathered and compared in this section.

# 4.1. Specimen design and fabrication

Similar to the configuration of the piecewise assembled Miura-ori array evaluated in Sec. 3.1 and 3.2, here the experimental specimen is assembled from one waterbomb unit cell at the center that interfaces with two arms of regular Miura-ori unit cells, Figure 7(a). Four unit cells of regular Miura-ori are on each side of the waterbomb tessellation. The facet dimensions are a = b = 60 mm,  $\gamma = 60^{\circ}$  for regular Miura-ori unit, and c = 60 mm, d = 30 mm for waterbomb unit. All the facets are made of corrugated polypropylene with overall thickness of 5 mm and flute pitch of 5 mm. The polypropylene sheets constituting the corrugated board are 0.3 mm thick. Each Miura-ori unit cell consists of four facets that are shaped by a laser cutter (Full Spectrum Laser, Las Vegas, NV). A circular miniature loudspeaker (Parts Express, Springboro, OH) is bonded at the center where a hole is laser cut to secure the speaker. The loudspeaker covers approximately 58% of the area of each facet. Detailed studies of the differences between model predictions and experimental data associated with the finite size of such active area compared to a model assumption of whole-facet sound radiation are given in (Zou and Harne, 2018). Six subfacets make up the waterbomb unit in the center to interface the regular Miura-ori on both sides. Threaded rods are inserted into the flutes to connect adjacent facets. All of the miniature loudspeakers are driven in parallel, while partial activation is realized by disconnecting desired loudspeakers.

# 4.2. Experiment setup

Experiments are undertaken in a hemi-anechoic acoustic chamber, with the dimensions  $7.78 \text{ m} \times 10.9 \text{ m} \times 4.66 \text{ m}$ . The specimen is affixed to fiberglass wedges to serve as a baffled backing. The folded angle of the

array is measured directly. A microphone (PCB Piezotronics, Depew, NY, 130E20) is used to measure the axial acoustic pressure of the array, as shown in Figure 7(b). A displacement sensor (WDS-1500-P60-SR-U, SN 51712) is used to directly measure the axial location of the microphone. A tonal signal is sent to an audio amplifier that drives the array. Data are post-processed in MATLAB.

# 4.3. Comparison between experimental and analytical results

Figure 8(a) presents the analytical results of axial acoustic pressure for the fully activated array when the amplitude of the normal surface velocity is 0.01 m/s. The normal surface velocity is empirically determined according to a fit of acoustic pressure amplitude with the analytical model, although normalized SPL values could likewise be used to eliminate the need for absolute value fitting (Jensen and Svendsen, 1992; Jimbo et al., 2016). Compared with the tessellated array samples considered in Sec. 3, here the experimental demonstrator is several times larger due to ease of fabrication and evaluation. As a result, the frequencies considered are scaled down proportionally with the longer acoustic wavelengths. For 1 kHz and folding angle is 37°, the axial acoustic pressure first increases along the axis, reaches a peak around R = 0.3 m and then decreases with increase in axial distance. While when the folding angle increases to 46°, Figure 8(a) shows that the SPL peak occurs near R = 0.25 m, with 2 dB greater SPL. A similar trend occurs at 3 kHz for the analytical results in Figure 8(a), while the focal range is more substantially reduced for the increased frequency of actuation. Figure 8(b) presents the corresponding experimental results. There is excellent qualitative agreement and good quantitative agreement for the case of 1 kHz and the folding angles 37° and 46° by comparing the measurements in Figure 8(b) to analytical predictions in Figure 8(a). The similar trends in change of focusing effects are likewise observed. There is less quantitative agreement between experiment and

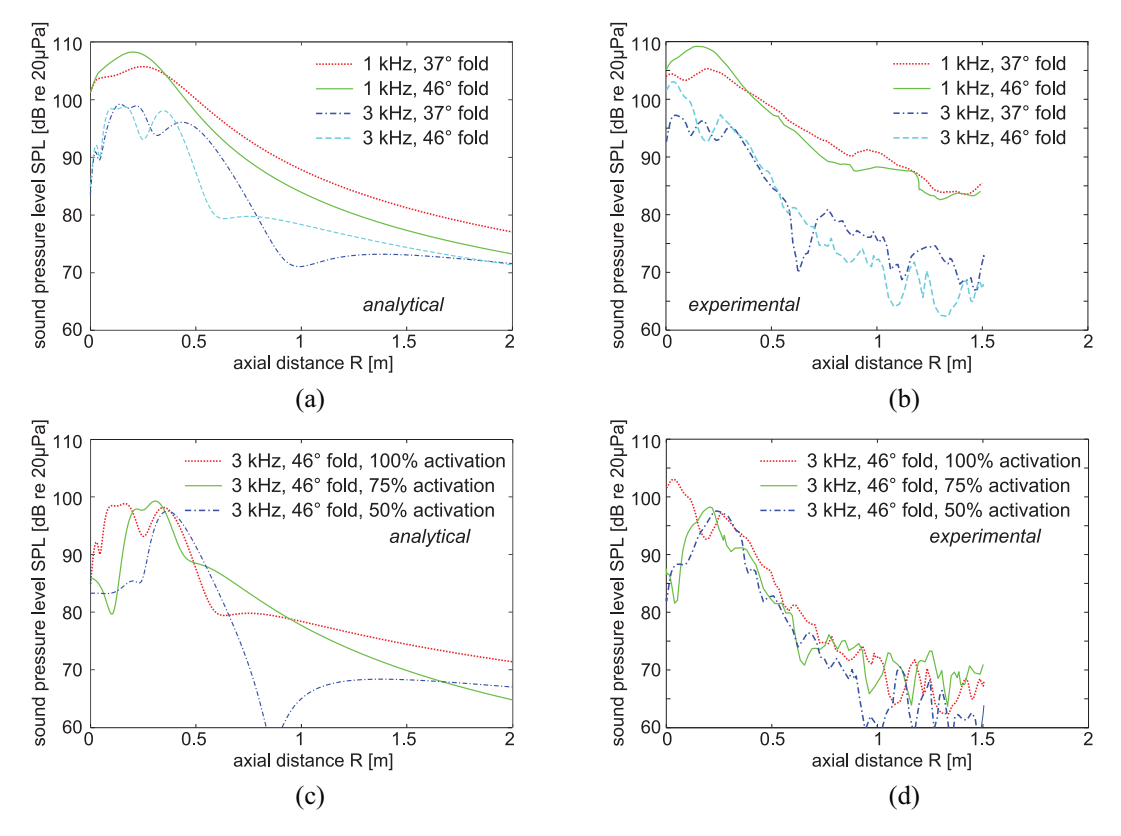


**Figure 8.** Comparison between experimental and analytical results of SPL as a function of axial distance: (a) shows the influence of folding angle on focusing behavior of the array when driven by two different frequencies, (b) experimental axial SPL, (c) analytical results of SPL as a function of axial distance when activation ratios are 100%, 75%, and 50%, and (d) experimental results of SPL as a function of axial distance when activation ratios are 100%, 75%, and 50%.

analysis for 3 kHz in Figure 8(a) and (b) due to the challenge of measuring shorter wavelengths more prone to diffraction against the facet surfaces (Zou and Harne, 2019), although the trends are present where a narrower focal range occurs for the more highly folded array. These findings verify that the more folded piecewise assembled array is more effective to focus sound in practice.

To examine the effectiveness of the partial activation approach to assist in focusing behavior, Figure 8(c) and (d) respectively compare analytical and experimental results of the array at 3 kHz when the activated surface contributions are changed. For Figure 8(c), by reducing the activation from 100% to 75% and to 50%, the focal point becomes more well defined and narrower in the 6 dB range around the peak. The similar quantitative and qualitative trends are observed in the experiments in Figure 8(d). Here, it is found that the fully activated array provides almost no focusing whereas the progressive reduction of activated array to 50% increases the focusing effect and tightens the focal range. These results explicitly confirm the hypotheses of this research through experimental practice. Given the verified extensibility of the partial activation approach to other acoustic array formulations, the potential is high for partially activated acoustic arrays to broaden the toolset of design for reconfigurable wave guiding structures.

### 5. Conclusions

This report explores a new concept of partially activating reconfigurable tessellated acoustic arrays in order to provide wave focusing capability to otherwise nonfocusing fully activated arrays. The analytical results show that a piecewise assembled array from Miura-ori and a waterbomb unit exemplify such capability although the advantages are limited in the frequency range. For this specific tessellated array, the focal point is both narrowed and enhanced in peak SPL by the reduction of the activated surface. Experiments on a similar tessellated array confirmed the qualitative and quantitative trends to support the new partial activation concept. Moreover, the approach was extended to a square twist-based acoustic array. In this case, the fully activated array showed no focusing behavior whereas a substantial focus was found for the array when only the square facets were activated. These concepts encourage designers to employ a broader range of parameters in the development of reconfigurable arrays for wave guiding than only the geometry and folding

extent of the tessellated structures. Looking ahead, opportunities may exist to improve upon the maintenance of shape so as to harness the full potential of the partial activation concept. By exploiting additional design and implementation factors, researchers may uncover new wave guiding functionality in reconfigurable structures.

### **Declaration of conflicting interests**

The author(s) declared no potential conflicts of interest with respect to the research, authorship, and/or publication of this article.

### **Funding**

The author(s) disclosed receipt of the following financial support for the research, authorship, and/or publication of this article: This project is supported by the National Science Foundation Faculty Early Career Development Award (No. 2054970).

#### **ORCID iD**

Ryan L Harne (b) https://orcid.org/0000-0003-3124-9258

#### References

- Alharbi S, Chaudhari S, Inahaar A, et al. (2018) E-textile origami dipole antennas with graded embroidery for adaptive RF performance. *IEEE Antennas and Wireless Propagation Letters* 17: 2218–2222.
- Babaee S, Overvelde JTB, Chen ER, et al. (2016) Reconfigurable origami-inspired acoustic waveguides. *Science Advances* 2: e1601019.
- Balanis CA (2016) Antenna Theory: Analysis and Design. Hoboken, NJ: Wiley.
- Belke CH and Paik J (2017) Mori: A modular origami robot. IEEE/ASME Transactions on Mechatronics 22: 2153–2164.
- Bertoldi K, Vitelli V, Christensen J, et al. (2017) Flexible mechanical metamaterials. *Nature Review Materials* 2: 17066.
- Bilgunde PN and Bond LJ (2018) Ultrasound beam characteristics of a symmetric nodal origami based array. *AIP Conference Proceedings* 1949: 080006.
- Boatti E, Vasios N and Bertoldi K (2017) Origami metamaterials for tunable thermal expansion. *Advanced Materials* 29: 1700360.
- Drinkwater BW and Wilcox PD (2006) Ultrasonic arrays for non-destructive evaluation: A review. NDT&E International 39: 525–541.
- Dudte LH, Vouga E, Tachi T, et al. (2016) Programming curvature using origami tessellations. *Nature Materials* 15: 583–588.
- Ebbini ES and Cain CA (1991) A spherical-section ultrasound phased array applicator for deep localized hyperthermia. *IEEE Transactions on Biomedical Engineering* 38: 634–643.
- Fink M, Montaldo G and Tanter M (2003) Time-reversal acoustics in biomedical engineering. *Annual Reviews of Biomedical Engineering* 5: 465–497.

Fuchi K, Tang J, Crowgey B, et al. (2012) Origami tunable frequency selective surfaces. *IEEE Antennas and Wireless Propagation Letters* 11: 473–475.

- Harker BM, Gee KL, Neilsen TB, et al. (2014) Phased-array measurements of full-scale military jet noise. In: *Proceedings of the 20th AIAA/CEAS aeroacoustics conference*, Atlanta, GA, 16–20 June, P.3069.
- Harne RL and Lynd DT (2016) Origami acoustics: Using principles of folding structural acoustics for simple and large focusing of sound energy. Smart Materials and Structures 25: 085031.
- Illing RO, Kennedy JE, Wu F, et al. (2005) The safety and feasibility of extracorporeal high-intensity focused ultrasound (HIFU) for the treatment of liver and kidney tumours in a Western population. *British Journal of Cancer* 93: 890.
- Jensen JA and Svendsen NB (1992) Calculation of pressure fields from arbitrarily shaped, apodized, and excited ultrasound transducers. IEEE Transactions on Ultrasonics, Ferroelectrics, and Frequency Control 39: 262–267.
- Jimbo H, Takagi R, Taguchi K, et al. (2016) Advantage of annular focus generation by sector-vortex array in cavitation-enhanced high-intensity focused ultrasound treatment. *Japanese Journal of Applied Physics* 55: 07KF19.
- Johnson M, Chen Y, Hovet S, et al. (2017) Fabricating biomedical origami: A state-of-the-art review. *International Journal of Computer Assisted Radiology and Surgery* 12: 2023–2032.
- Kennedy JE (2005) High-intensity focused ultrasound in the treatment of solid tumours. *Nature Reviews Cancer* 5: 321–327.
- Kinsler LE, Frey AR, Coppens AB, et al. (2000) *Fundamentals of Acoustics*. New York, NY: John Wiley and Sons.
- Kuribayashi K, Tsuchiya K, You Z, et al. (2006) Self-deployable origami stent grafts as a biomedical application of Nirich TiNi shape memory alloy foil. *Materials Science and Engineering:* A 419: 131–137.
- Liu X, Yao S, Cook BS, et al. (2015) An origami reconfigurable axial-mode bifilar helical antenna. *IEEE Transactions on Antennas and Propagation* 63: 5897–5903.
- Lv C, Krishnaraju D, Konjevod G, et al. (2014) Origami based mechanical metamaterials. *Scientific Reports* 4: 5979.
- Martinez RV, Fish CR, Chen X, et al. (2012) Elastomeric origami: Programmable paper-elastomer composites as pneumatic actuators. *Advanced Functional Materials* 22: 1376–1384.
- Miyashita S, Guitron S, Li S, et al. (2017) Robotic metamorphosis by origami exoskeletons. *Science Robotics* 2: eaao4369.
- Ocheltree KB and Frizzell LA (1989) Sound field calculation for rectangular sources. *IEEE Transactions on Ultrasonics*, *Ferroelectrics*, and Frequency Control 36: 242–248.
- O'Neil HT (1949) Theory of focusing radiators. *The Journal of the Acoustical Society of America* 21: 516–526.
- Overvelde JTB, De Jong TA, Shevchenko Y, et al. (2016) A three-dimensional actuated origami-inspired transformable metamaterial with multiple degrees of freedom. *Nature Communications* 7: 10929.

- Ross AB, Diederich CJ, Nau WH, et al. (2005) Curvilinear transurethral ultrasound applicator for selective prostate thermal therapy. *Medical Physics* 32: 1555–1565.
- Rus D and Tolley MT (2018) Design, fabrication and control of origami robots. *Nature Reviews Materials* 3: 101–112.
- Schenk M and Guest SD (2011) Origami folding: A structural engineering approach. In: Wang-Iverson P, Lang RJ and Yim M (eds) *Origami 5: Fifth International Meeting of Origami Science, Mathematics, and Education.* Boca Raton, FL: CRC Press, pp.291–304.
- Schenk M and Guest SD (2013) Geometry of Miura-folded metamaterials. Proceedings of the National Academy of Sciences 110: 3276–3281.
- Sessions D, Fuchi K, Pallampati S, et al. (2018) Investigation of fold-dependent behavior in an origami-inspired FSS under normal incidence. *Progress In Electromagnetics Research* 63: 131–139.
- Silverberg JL, Evans AA, McLeod L, et al. (2014) Using origami design principles to fold reprogrammable mechanical metamaterials. *Science* 345: 647–650.
- Tachi T (2010) Geometric considerations for the design of rigid origami structures. In: *Proceedings of the international* association for shell and spatial structures, Shanghai, China, 8–12 November, pp.458–460.

- Wan H, VanBaren P, Ebbini ES, et al. (1996) Ultrasound surgery: Comparison of strategies using phased array systems. IEEE Transactions on Ultrasonics, Ferroelectrics, and Frequency Control 43: 1085–1098.
- Williams EG (1999) Fourier Acoustics: Sound Radiation and Nearfield Acoustical Holography. San Diego, CA: Academic Press.
- Yao S, Liu X and Georgakopoulos SV (2017) Morphing origami conical spiral antenna based on the Nojima wrap. *IEEE Transactions on Antennas and Propagation* 65: 2222–2232.
- Zou C and Harne RL (2017) Adaptive acoustic energy delivery to near and far fields using foldable, tessellated star transducers. *Smart Materials and Structures* 26: 055021.
- Zou C and Harne RL (2018) Piecewise assembled acoustic arrays based on reconfigurable tessellated structures. *Journal of the Acoustical Society of America* 144: 2324–2333.
- Zou C and Harne RL (2019) Tailoring reflected and diffracted wave fields from tessellated acoustic arrays by origami folding. *Wave Motion* 89: 193–206.
- Zou C, Lynd DT and Harne RL (2018) Acoustic wave guiding by reconfigurable tessellated arrays. *Physical Review Applied* 9: 014009.